UC Berkeley
UC Berkeley Previously Published Works

Title
Investigating the Binarity of S0-2: Implications for Its Origins and Robustness as a Probe of the Laws of Gravity around a Supermassive Black Hole

Permalink
https://escholarship.org/uc/item/8s67j8n7

Journal
The Astrophysical Journal, 854(1)

ISSN
0004-637X

Authors
Chu, Devin S
Do, Tuan
Hees, Aurelien
et al.

Publication Date
2018-02-10

DOI
10.3847/1538-4357/aaa3eb

Peer reviewed

INVESTIGATING THE BINARITY OF S0-2: IMPLICATIONS FOR ITS ORIGINS AND ROBUSTNESS AS A PROBE OF THE LAWS OF GRAVITY AROUND A SUPERMASSIVE BLACK HOLE

Devin S. Chu[1], Tuan Do[1], Aurelien Hees[1], Andrea Ghez[1], Smadar Naoz[1], Gunther Witzel[1], Shoko Sakai[1], Samantha Chappell[1], Abhimat K. Gautam[1], Jessica R. Lu[2], Keith Matthews[3]

Draft version December 20, 2017

ABSTRACT

The star S0-2, which orbits the supermassive black hole (SMBH) in our Galaxy with a period of 16 years, provides the strongest constraint on both the mass of the SMBH and the distance to the Galactic center. S0-2 will soon provide the first measurement of relativistic effects near a SMBH. We report the first limits on the binarity of S0-2 from radial velocity monitoring, which has implications for both understanding its origin and robustness as a probe of the central gravitational field. With 87 radial velocity measurements, which include 12 new observations presented, we have the data set to look for radial velocity variations from S0-2's orbital model. Using a Lomb-Scargle analysis and orbit fitting for potential binaries, we detect no radial velocity variation beyond S0-2's orbital motion and do not find any significant periodic signal. The lack of a binary companion does not currently distinguish between different formation scenarios for S0-2. The upper limit on the mass of a companion star ($M_{\rm comp}$) still allowed by our results has a median upper limit of $M_{\rm comp} \sin i \leq 1.6$ $M_\odot$ for periods between 1 and 150 days, the longest period to avoid tidal break up of the binary. We also investigate the impact of the remaining allowed binary system on the measurement of the relativistic redshift at S0-2's closest approach in 2018. While binary star systems are important to consider for this experiment, we find plausible binaries for S0-2 will not alter a 5σ detection of the relativistic redshift.

Subject headings: Galaxy: center — stars: early-type — techniques: high angular resolution — gravitation

1. INTRODUCTION

The source S0-2 is one of the most well studied stars at the Galactic center. It is important for our understanding of the properties of the Galaxy's central potential. In particular, it has provided the proof of the existence of a supermassive black hole (SMBH), the characterization of the SMBH properties (mass and distance) and the laws of gravitation (Ghez et al. 2005, 2008; Gillessen et al. 2009b, 2017; Boehle et al. 2016; Hees et al. 2017). S0-2 is also notable because spectroscopic studies have revealed that it, along with most of the "S-stars" located within 1″ of the black hole, is a young main-sequence B star (Ghez et al. 2003; Eisenhauer et al. 2005; Martins et al. 2008; Habibi et al. 2017). This discovery raised questions about their formation mechanism, since traditional star formation would be disrupted by the tidal forces of the black hole (Morris 1993).

Works have investigated ways the S-stars may have formed and how these stars relate to the rest of the nuclear star cluster. Many theories for the S-stars' formation have been proposed (see Alexander 2005, for a review). Two general classifications of mechanisms are considered for the S-stars: (1) binary star systems scattered from outside the region and then tidally disrupted, leaving behind one component of the original binary while the other is ejected as a hypervelocity star (Hills 1988; Perets et al. 2007), and (2) S-stars formed in the clock-wise disk and then migrated to the central arcsecond around the SMBH (Levin 2007; Löckmann et al. 2008; Merritt et al. 2009). Previous works have also investigated how these S-stars relate to the clockwise disk, Wolf-Rayet stars, G2-like sources and evolved giants in the region (Paumard et al. 2006; Lu et al. 2009; Bartko et al. 2009; Do et al. 2009, 2013; Madigan et al. 2014; Chen & Amaro-Seoane 2014; Witzel et al. 2014, 2017; Phifer et al. 2013).

With binary stars playing a leading role in many of the S-star formation and evolution scenarios as well as in scenarios of other Galactic center stars, observational searches for binaries are important. Thus far, photometric variations has been the primary search method. Several binaries have been revealed (Ott et al. 1999; Martins et al. 2006; Rafelski et al. 2007; Pfuhl et al. 2014), although none among the S-stars. However, eclipsing binaries are expected to be only a small fraction of the true binary population. With radial velocity (RV) measurements that now span more than a decade, there is an opportunity to search for RV variations in the brightest S-star cluster members.

Furthermore, S0-2 will be at its closest approach to the SMBH in 2018, which provides the opportunity to measure the relativistic redshift in S0-2's RV (Zucker et al. 2006; Angélil & Saha 2010, 2011; Hees et al. 2017). This first direct observation of a relativistic effect on S-stars orbit will improve with time after 2018 and be followed by other relativistic measurement such as the advance of the periastron. If S0-2 is actually a spectroscopic binary, it will bias the relativistic redshift measurement if binarity is not considered.

In this work, we explore the possibility of S0-2 to be a

[1] Department of Physics and Astronomy, University of California, Los Angeles, CA 90095, USA
[2] Astronomy Department, University of California, Berkeley, CA 94720, USA
[3] Division of Physics, Mathematics, and Astronomy, California Institute of Technology, Pasadena, CA 91125, USA

spectroscopic binary. This paper is organized as follows: In Section 2 we describe the observations and data used in this work, including new RV measurements. Section 3 describes the search for a companion star and the characterization of allowed hidden companions. Section 4 describes the impact allowed spectroscopic binaries would have on the relativistic redshift measurement. Section 5 interprets the results of the analysis and implications for S0-2 being a single star and the robustness of gravitational redshift measurements and future relativity studies based on S0-2's orbital motion.

2. OBSERVATIONS AND DATA

This investigation includes previously reported astrometric and spectroscopic data, as well as new spectroscopic data taken with the W. M. Keck Observatory (WMKO). All the WMKO spectroscopic observations used for S0-2 RV measurements are summarized in Table 1.

2.1. S0-2 Radial Velocities

2.1.1. Previously Reported Data

Over the past 16 years, S0-2 has been closely monitored spectroscopically. In the published literature, 24 RV measurements beginning in the year 2000 have been reported from WMKO (Ghez et al. 2003, 2005, 2008; Boehle et al. 2016) and 40 measurements beginning in 2003 from the VLT (Eisenhauer et al. 2005; Gillessen et al. 2009a, 2017; Habibi et al. 2017). Many of the RV measurements are based on multiple nights of observations. For this analysis, we are interested in the presence of binaries, which for S0-2 can have periods as short as ∼1 day. We therefore reextract S0-2's spectra from the previously calibrated WMKO data on a nightly basis for the following nights which were previously combined: 2009 May 5 and 6 to 2009.334, 2010 May 5 and 8 to 2010.349, 2012 June 8-11 to 2012.441, 2012 July 21 and 22 to 2012.556, 2012 August 12 and 13 to 2012.616, 2013 May 14 and 16 to 2013.369, 2013 July 25-27 to 2013.566, and 2013 August 10-13 to 2013.612 (see Table 1). This increases the Keck data set to 38 points for this time period. For the VLT, 7 out of 41 epochs are reported to be derived from multiple nights of data.

2.1.2. New Spectroscopic Data

We report new spectroscopic observations for S0-2 obtained using the integral field spectrograph OSIRIS (Larkin et al. 2006) on the W. M. Keck I telescope with the laser guide star AO system. These data were observed between 2014 to 2016. Details about the filters and integration time relate to these observations are given in Table 1. The RV observations and data analysis follow the same procedures used for earlier WMKO S0-2 RV measurements (Ghez et al. 2008; Do et al. 2013). The 8 new RV measurements, along with the RV measurements from Section 2.1.1 (38 Keck and 41 VLT) result in 87 total RV measurements used in this work (see Table 3).

2.2. Characteristics of the Two Datasets

The Keck and VLT data sets are analyzed in a similar manner and appear to be consistent with one another. The two datasets are analyzed with the same

standard spectroscopic calibration procedures and the absolute wavelength solutions are both determined from the OH sky emmision lines. The radial velocity of S0-2 is measured from both data sets by fitting a Gaussian to the Brγ absorption line. The reported average RV uncertainties are very similar, 33 km s^{-1} and 45 km s^{-1} for Keck and VLT, respectively. Furthermore, for the 4 Keck and VLT points taken within 10 days of each other, 3 of the points were within 1σ of each other. The one exception is the Keck 2003.433 point, which differs from a nearby VLT point by 2σ. We conclude there is no significant systematic difference.

2.3. Removing S0-2's Long-term RV Variations

Before searching for short-term RV variations, we remove the long-term RV variations from S0-2's orbital motion around the SMBH. To create the long-term RV model, a simultaneous orbital fit of S0-2 and S0-38 was performed using the same S0-2 and S0-38 astrometry and process as Boehle et al. (2016), but with the S0-2 RVs in Table 3 and S0-38 RVs from Boehle et al. (2016); Gillessen et al. (2017). One additional change is the format of time used. In this work, we use Modified Julian Date (MJD). The reported time is the approximate average time of the observations taken during the night. For convenience, we also report the Universal Time (UT) and epoch time reported in Julian years of 365.25 days since J2000. Previously, Boehle et al. (2016) defined the epoch year as 365.24 days. The orbital parameters resulting from the fit are consistent with Boehle et al. (2016) within 1σ and are presented in the Appendix A. The RV data, model and residual are shown in Figure 1 and given in Table 3. The average scatter around the orbit residual is 20 km s^{-1} with a standard deviation of 26 km s^{-1}. The Keck and VLT datasets are individually consistent with these values.
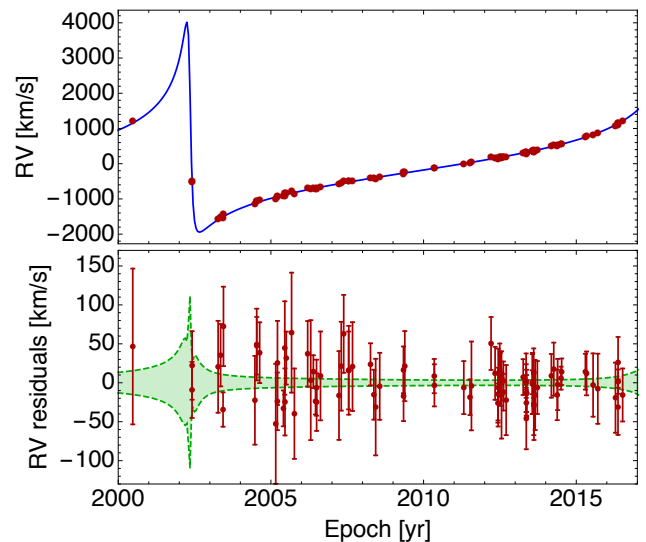

FIG. 1.— Top: S0-2's radial velocity measurements over time and best fit model. Bottom: Residual radial velocity curve. Dashed lines are the 1σ model uncertainties.

3. IS S0-2 A BINARY?

TABLE 1
Summary of Keck Spectroscopic Observations

Date			$N_{\mathrm{frames}} \times t_{\mathrm{int}}$	FWHM [a]	Filter	Scale
(UT)	(MJD)	(Epoch)	(s)	(mas)		(mas)
2000-06-23	51718.50	2000.476	36×300		K [b]	18
2002-06-02	52427.50	2002.418	7×1200		K [c]	20
2002-06-03	52428.50	2002.420	4×1200		K' [c]	20
2003-06-08	52798.50	2003.433	2×1200		K' [c]	20
2004-06-23	53179.50	2004.476	16×1200		K' [c]	20
2005-05-30	53520.50	2005.410	7×1200		K' [c]	20
2005-07-03	53554.50	2005.503	7×900	58	Kbb	20
2006-05-23	53878.50	2006.390	4×900	74	Kbb	35
2006-06-18	53904.50	2006.461	9×900	65	Kn3	35
2006-06-30	53916.50	2006.494	9×900	59	Kn3	35
2006-07-01	53917.50	2006.497	9×900	64	Kn3	35
2007-05-21	54241.50	2007.384	2×900	86	Kn3	35
2007-07-19	54300.29	2007.545	2×900	56	Kn3	35
2008-05-16	54602.50	2008.372	11×900	57	Kn3	35
2008-07-25	54672.28	2008.563	9×900	60	Kn3	35
2009-05-05	54956.50	2009.342	7×900	60	Kn3	35
2009-05-06	54957.50	2009.344	12×900	69	Kn3	35
2010-05-05	55321.50	2010.341	6×900	67	Kn3	35
2010-05-08	55324.50	2010.349	11×900	69	Kn3	35
2011-07-10	55752.33	2011.520	6×900	71	Kn3	35
2012-06-08	56086.50	2012.435	4×900	87	Kn3	35
2012-06-09	56087.50	2012.438	3×900	66	Kn3	35
2012-06-11	56089.50	2012.444	7×900	64	Kn3	20
2012-07-21	56129.31	2012.553	3×900	77	Kn3	35
2012-07-22	56130.31	2012.555	7×900	81	Kn3	35
2012-08-12	56151.33	2012.613	6×900	56	Kn3	35
2012-08-13	56152.27	2012.615	7×900	99	Kn3	35
2013-05-11	56423.50	2013.358	11×900	73	Kbb	35
2013-05-12	56424.50	2013.361	11×900	62	Kbb	35
2013-05-13	56425.50	2013.363	12×900	61	Kbb	35
2013-05-14	56426.50	2013.366	11×900	61	Kn3	35
2013-05-16	56428.50	2013.372	7×900	98	Kn3	20
2013-05-17	56429.50	2013.374	7×900	64	Kn3	20
2013-07-25	56498.33	2013.563	11×900	79	Kn3	35
2013-07-26	56499.34	2013.566	6×900	73	Kn3	35
2013-07-27	56500.33	2013.568	11×900	66	Kn3	35
2013-08-10	56514.29	2013.607	7×900	62	Kn3	35
2013-08-11	56515.31	2013.609	9×900	69	Kn3	35
2013-08-13	56517.29	2013.615	12×900	67	Kn3	35
2014-05-18	56795.50	2014.376	13×900	66	Kn3	35
2014-05-23	56800.50	2014.390	10×900	76	Kn3	35
2014-07-03	56841.36	2014.502	8×900	66	Kn3	35
2015-05-04	57146.50	2015.337	5×900	68	Kn3	35
2015-07-21	57224.35	2015.551	5×900	56	Kn3	35
2016-05-14	57522.50	2016.367	8×900	78	Kbb	35
2016-05-15	57523.50	2016.370	4×900	80	Kbb	35
2016-05-16	57524.50	2016.372	8×900	84	Kbb	35

[a] Average FWHM of S0-2 in the mosaic made of all frames, measured by fitting a two-dimensional Gaussian to the source.
[b] Taken with NIRSPEC slit spectrograph
[c] Taken with NIRC2 slit spectrograph

In this section, we use two different methods to to search for periodic signals in the RV residuals: (i) the Lomb-Scargle periodogram (Lomb 1976; Scargle 1982; Astropy Collaboration et al. 2013) and (ii) a Bayesian fit for potential binaries. The former method provides quick overview of the data; we note that while it may not be as effective at detecting highly eccentric binaries (e.g. phase dispersion measure (Stellingwerf 1972), minimum string length (Dworetsky 1983)), it is an computationally efficient method for detecting periodic signals in un-evenly spaced data (see Appendix B). The latter method provides a more complete and robust, albeit more computationally expensive approach and allows us to derive upper limits on the orbital parameters of an hypothetical binary companion to S0-2.

We can place an upper limit on the orbital period of any possible companion around S0-2 of 119.2 days based on a binary disruption criteria. A binary would be tidally disrupted at closest approach to the SMBH if it has a separation greater than the Hill radius (r_{H}). The Hill radius is given by

$$r_{\mathrm{H}} = a_{\mathrm{S0\text{-}2}}(1 - e_{\mathrm{S0\text{-}2}}) \sqrt[3]{\frac{M_{\mathrm{Primary}}}{3 M_{BH}}}, \qquad (1)$$

where M_{Primary} is the primary mass, $a_{\mathrm{S0\text{-}2}}$ and $e_{\mathrm{S0\text{-}2}}$ are the semimajor axis and eccentricity for the binary-black hole system (the corresponding values have been derived from the orbital fit presented in Section 2.3 whose result is presented in Appendix A). This Hill Radius limit is

a conservative limit since any eccentricity of the inner binary system would decrease the stability of the system. We take the condition $a(1 + e) < r_H$, where e is the eccentricity and a the semi-major axis of the inner binary, to allow for longterm stability (Naoz 2016), which leads to the following constraint on the binary period P

$$P^2 < \frac{4\pi^2}{3GM_{BH}} a_{S0\text{-}2}^3 \frac{(1 - e_{S0\text{-}2})^3}{(1 + e)^3} \frac{M_{\text{Primary}}}{M_{tot}} . \quad (2)$$

This condition needs to be fulfilled to avoid a disruption of the binary. We therefore sampled periods between 1 and 150 days to search for a significant periodic signal.
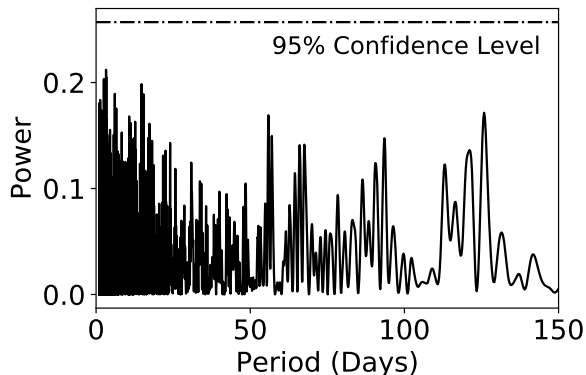
Fig. 2.— Lomb-Scargle periodogram of S0-2's residual RV curve. The black dash-dotted line is the 95% confidence level detection value. No power reaches the 95% confidence level detection value implying that no significant periodic signal is found in the observations.

The Lomb-Scargle analysis on S0-2's RV does not reveal any statistically significant peak (see Figure 2). We note that the structure of this periodogram is unaffected by the model uncertainties over the period range searched. In order to determine the relationship between periodogram power and statistical significance, we ran a series of Monte Carlo simulations. We first generated 100,000 simulated residual RV curves with no periodic signal. The simulated points had the same observation times and uncertainties as the data and were drawn from a Gaussian centered around 0 km s^{-1}. We produced a periodogram for each simulated RV curve and found the maximum peak power value. We then looked at the distribution of these maximum power values and made a cumulative distribution function (CDF). We used this CDF to determine the significance for periodic detections. These simulations set the 95% confidence level detection limit to be 0.25, shown in a dotted line in Figure 2. The periodogram corresponding to S0-2's observations never reaches this value, which implies that no significant periodic signal is found in the current data and that observations are consistent with a single star model.

Since no evidence of a binary for S0-2 is found, we can place an upper limit on the amplitude on the RV variations induced by a binary system. In order to infer such a limit, we fit the S0-2 RV residuals with a binary star RV model plus a constant. The following equation was used to model the RV curve of an eccentric binary

system (Hilditch 2001)

$$RV = K \frac{\sqrt{1 - e^2} \cos E \cos \omega - \sin E \sin \omega}{1 - e \cos E} , \quad (3)$$

with

$$K = \frac{2\pi a \sin i}{P} , \quad (4)$$

and where e is the binary eccentricity, ω the argument of periastron, E the eccentric anomaly determined by solving the Kepler equation, i the inclination, P the period and a the semimajor axis. This model is parametrized using the following 5 variables: the offset O, the RV amplitude K, the eccentricity e, the argument of periastron ω and the mean longitude at J2000 (noted L_0). The use of the mean longitude at J2000 is preferred to the usual time of closest approach which is not bounded and not defined in case of circular orbits (Hilditch 2001). For different fixed binary orbital periods P, we fitted this model to the RV residuals using a MULTINEST sampler (Feroz & Hobson 2008; Feroz et al. 2009, 2013). The resulting 95% upper confidence limit on K for $\sim$3000 orbital periods ranging from 1 to 150 days is shown in Figure 3.
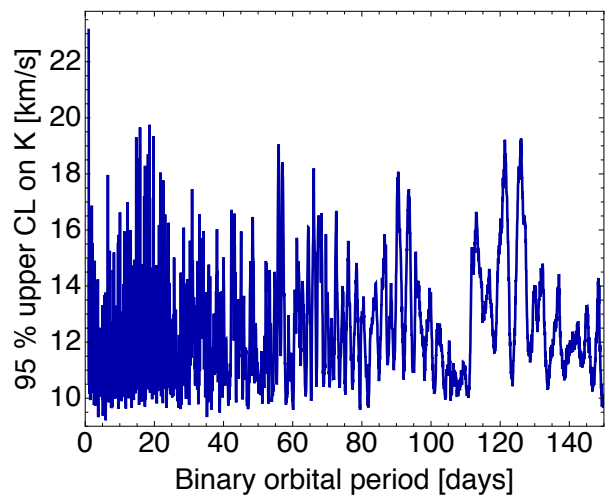

Fig. 3.— Upper limits on the amplitude of RV variations induced by possible undetected companion stars. Plotted at the 95% upper confidence limit, the amplitude of RV variations that could be induced by a hidden binary system (K as defined by equations 3 and 4) as a function of the binary orbital period.

Like the Lomb-Scargle analysis, this method is also sensitive to periodic signals in the data. A periodic signal would yield a significant non-zero peak in the value of K in the posterior, as opposed to a power law decreasing posterior. This method also takes inherently into account the other orbital parameters of the binary system that can affect the shape of the curve (e.g. eccentricity).

With one further assumption, this analysis also allows us to constrain the mass of a hypothetical companion. Assuming a total mass of the system (M_{tot}), we transform the sampling (i.e. the chain) resulting from the MULTINEST run into a companion mass limit by using

$$M_{\text{comp}} \sin i = \left(\frac{P M_{tot}^2}{2\pi G} \right)^{1/3} K , \quad (5)$$

where M_{comp} is the companion mass and i the inclination of the binary system. From this transformed chain, we can derive an upper 95% confidence limit on $M_{\text{comp}} \sin i$. This limit depends on the total mass M_{tot} used in Equation 5. In this work, two extreme values for M_{tot} are considered: (i) a low value of $M_{\text{tot}} = 10$ M$_\odot$ (Habibi et al. (2017) reported the mass of S0-2 as $13.6^{+2.2}_{-1.8}$ M$_\odot$) and (ii) a high value of $M_{\text{tot}} = 20$ M$_\odot$. The upper limit on $M_{\text{comp}} \sin i$ is shown in Figure 4 as well as the excluded region inferred by theoretical arguments based on the on the binary disruption criteria[4] and characterized by equation 2. The median upper 95% confidence limit for $M_{\text{comp}} \sin i$ for all periods is 1.6 M$_\odot$ assuming a total mass of 20 M$_\odot$ while its maximal value is 2.8 M$_\odot$ at 93.5 days period. These values decrease by 36 % for a total mass M_{tot} of 10.0 M$_\odot$.

4. IMPACT OF HIDDEN ALLOWED COMPANIONS ON MEASUREMENT OF S0-2'S RELATIVISTIC REDSHIFT

As anticipated by many theorists, observations of short-period stars orbiting the SMBH in our Galactic center are currently opening a new window to test the gravitational theory and to measure relativistic effects (see e.g. Rubilar & Eckart (2001); Zucker et al. (2006); Will (2008); Borka et al. (2013); Zakharov et al. (2016); Johannsen (2016a,b); Psaltis et al. (2016); Hees et al. (2017); Iorio (2017) and references therein). The relativistic redshift on S0-2's RV is the first relativistic effect expected to be detected with S0-2's closest approach in 2018 (Zucker et al. 2006; Angélil & Saha 2010, 2011; Hees et al. 2017). This measurement of the relativistic redshift will improve with time in the future and will also be followed by measurements of more relativistic effects such as the advance of S0-2's periastron. In the case where S0-2 is a binary system, the measurement of the relativistic effects like the redshift would be altered. The goal of this section is to quantify the impact of a binarity of S0-2 on the measurement of its relativistic redshift.

One way to measure the relativistic redshift is to model the total RV as $RV = [RV]_{\text{Newton}} + \Upsilon [RV]_{\text{rel}}$, where $[RV]_{\text{Newton}}$ is the standard Newtonian RV, Υ a dimensionless parameter whose value is equal to 1 in GR and $[RV]_{\text{rel}}$ is the first order relativistic contribution to the RV given by

$$[RV]_{\text{rel}} = \frac{v^2}{2c} + \frac{GM_{BH}}{rc}, \qquad (6)$$

with c the speed of light in a vacuum and r the norm of the star's position with respect to the SMBH and v the norm of its velocity. The first term is a contribution due to special relativity while the second term corresponds to the gravitational redshift. For a Keplerian orbit, the two contributions are exactly the same (up to a constant factor), meaning that only their combination can be measured. The relativistic redshift contribution to S0-2's RV reaches 200 km/s at closest approach in 2018 while the Newtonian part is ranging from -2000 km/s to 4000 km/s (see Figure 1). The idea is to fit Υ simultaneously with the other parameters in the orbital fit: a value signifi-

TABLE 2
IMPACT OF A BINARITY OF S0-2 ON A MEASUREMENT OF THE RELATIVISTIC REDSHIFT.

Binary period	95 % C.L. on K [km/s] [a]	Uncertainty on the redshift due to the binarity (σ_Υ)
2 days	16.0	0.031
5 days	10.4	0.011
10 days	12.2	0.026
25 days	12.6	0.051
50 days	11.0	0.036
100 days	12.9	0.039

[a] K is the amplitude of the RV variations induced by a binary as introduced in equations 3 and 4. The 95 % upper confidence limits on K are presented on Figure 3.

cantly different from 0 but compatible with 1 would be a successful detection of the relativistic redshift while a value significantly different from 1 would indicate a deviation from GR. The goal of this section is to quantify the impact of a plausible binary for S0-2 on the determination of Υ.

The methodology consists in simulating data assuming S0-2 is a binary star using a relativistic modeling (in particular we use $\Upsilon = 1$) and analyze these data using a modeling where S0-2 is a single star and where Υ is a free parameter. The deviation $\Upsilon - 1$ obtained in this analysis is therefore entirely due to the fact that S0-2 has been simulated as a binary star.

More precisely, we simulate astrometric and RV data for S0-2 using a relativistic modeling that includes the Römer time delay and the redshift (see e.g. Alexander (2005)). The simulated epochs correspond to epochs where we actually have data (see Table 3) and for each simulated data, we assign an uncertainty that corresponds to the actual measurement. In addition to existing data, we included simulated data for 2018: 10 spectroscopic observations which were assigned an uncertainty of 25 km/s and 4 astrometric observations which were assigned an uncertainty of 0.3 mas. The epochs for these additional observations have been chosen to optimize a redshift measurement within the 2018 observation window. At this step, the simulated data corresponds to perfect measurements in the case where S0-2 is a single star. Therefore, an orbital fit using these simulated data recovers the input value, i.e. gives an estimate of $\Upsilon = 1$ as expected.

To these simulated data, we then add the signature produced by a binary star given by Eq. (3). The obtained data now corresponds to a binary system. This dataset is then used in a one star orbital fit that includes the GM_{BH}, the distance to our Galactic center R_0, the position and velocity of the BH, the 6 orbital parameters for the star and the relativistic redshift parameter Υ. The impact of the binarity of S0-2 on the redshift measurement will be given by the estimated value[5] of $\Upsilon - 1$.

This procedure has been performed for 6 different binary orbital periods: 2, 5, 10, 25, 50 and 100 days. For each of these periods, we draw 2000 samples for the other binary orbital parameters (eccentricity e, RV amplitude K, argument of periastron ω and longitude at J2000 L_0)
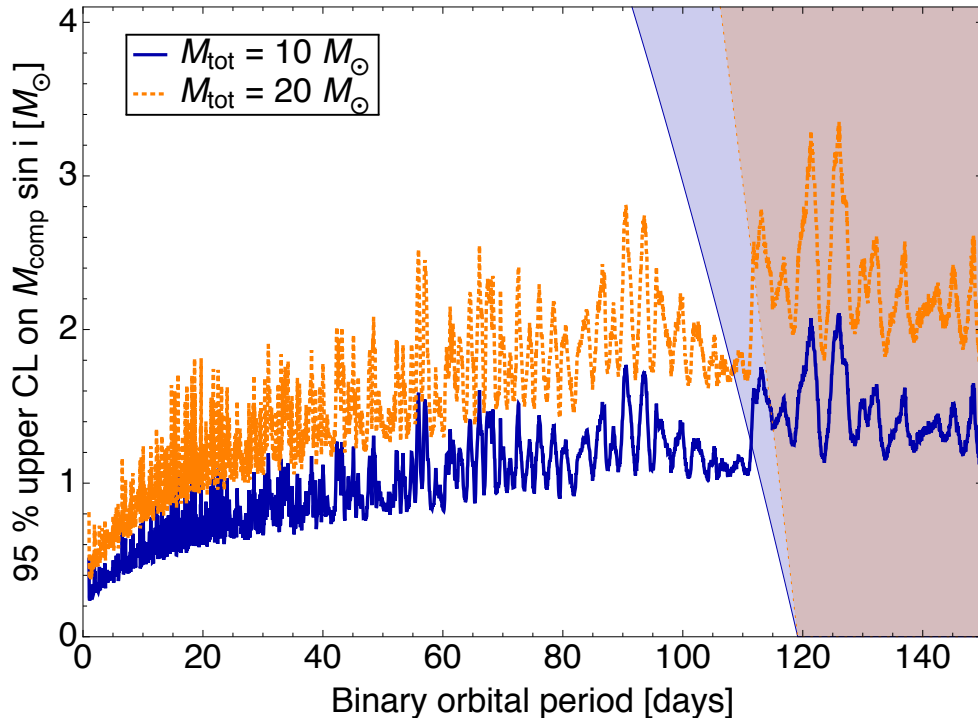
Fig. 4.— Upper limits on allowed companion star masses. Plotted are the 95% upper confidence limits on $M_{comp} \sin i$ as a function of the binary orbital period assuming two different values for the total mass of the binary system. The shaded regions represent the area excluded by the Hill radius limits from equation 2 while adopting a circular orbit (which corresponds to the most conservative limit).
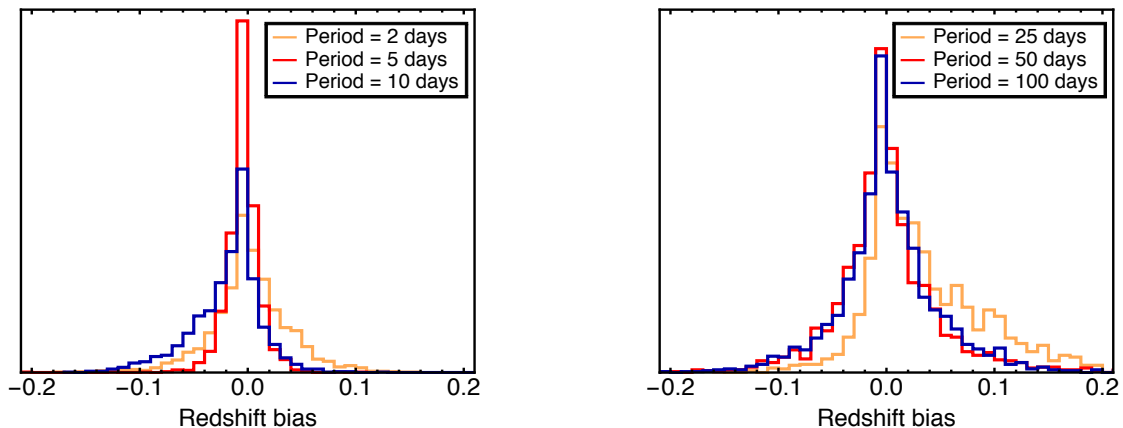

Fig. 5.— Bias on the estimation of relativistic redshift ($\Upsilon - 1$). Plotted are the imposed biases from model fits using simulated S0-2 observations, which extend through 2018 and which include RV variations induced by binary stars systems allowed by the current S0-2 RV data. The different curves correspond to different binary periods. In general, the periods that have stricter companion limits, result in smaller biases; the median binary amplitude limits correspond to a redshift bias of 0.03.

from the posterior probability distribution function of the fit described in Section 3. The resulting distributions for the bias in the redshift measurement $\Upsilon - 1$ are presented in Fig. 5. Furthermore, the values of the half of the 68% upper limit on the absolute value of the redshift bias are given in Tab. 2. In general, the periods that have stricter limits on the amplitude of the RV variations (K) induced by a hidden binary, result in smaller biases; the median binary amplitude limits correspond to a redshift bias of 0.03.

Although a plausible binary for S0-2 can bias the measurement of the relativistic redshift, this bias is always smaller than the uncertainty corresponding to a 5σ detection of the redshift (a 5σ detection is characterized by $\sigma_\Upsilon = 0.2$).

5. DISCUSSION AND CONCLUSION

5.1. *S0-2 in its astrophysical context*

This is the first work that investigates S0-2 as a spectroscopic binary. Previous searches have concentrated on

brighter sources such as IRS16SW and E60 (Pfuhl et al. 2014), located beyond the S-star cluster region (outside of ∼0.04 pc). This work has pushed the RV searches to 2 magnitudes fainter from K = 12.0 (E60) down to K = 14.0; physically, this magnitude difference corresponds to the difference between evolved Wolf-Rayet stars and main-squence B stars. The improvements here are driven by the large number of RV measurements available for S0-2 from the long-baseline monitoring programs for this source (e.g., Boehle et al. 2016; Gillessen et al. 2017).

While we detect no significant binary signal in the RV variations, we have been able to place stringent limits on the companion mass. Our limits of 1.6 $M_\odot$ are consistent with other observations of the star. For example, given our 95% confidence limit of 1.6 $M_\odot$, a star would have an observed brightness of K ∼ 18 mag at the Galactic center, corresponding to a factor of 40 times less flux than S0-2. This brightness ratio is consistent with the fact that S0-2's spectrum shows no sign of another set of spectral features, even with 10 years of spectra combined (Habibi et al. 2017). While our mass limits has a $\sin i$ degeneracy, the lack of detection of a double-lined source also shows that a face-on binary system is also very unlikely.

The lack of a binary companion does not distinguish between different formation scenarios for S0-2 at this time. No companion is expected if S0-2 is the remaining companion of a hypervelocity star (e.g. Hills 1988; Yu & Tremaine 2003; Perets et al. 2009), or if it is the product of a merger (e.g. Sana et al. 2012; Phifer et al. 2013; Witzel et al. 2014; Stephan et al. 2016). Scattering from the young star cluster (at 0.1 to 0.5 pc) could also bring S0-2 in without a companion (Perets et al. 2007; Madigan et al. 2014). While the current observations of S0-2 are unable to distinguish these scenarios, companion searches of the other S-stars should be able to provide a much more comprehensive test of the formation scenarios for the S-stars. We have concentrated on S0-2 because the other S-stars are all fainter, which results in lower precision in their RV compared to S0-2. Additional measurements should improve the sensitivity of companion searches.

5.2. *S0-2 as a new probe of fundamental physics*

The relativistic redshift at S0-2's closest approach in 2018 will be the first measurement of its kind, so understanding all sources of bias will be especially important for a significant detection. We have shown that a binary companion below our current detection limit for S0-2 can bias this measurement, as shown in Sec. 4. Nevertheless, this bias is always smaller than the uncertainty corresponding to a 5σ detection of the redshift. The values reported in Tab. 2 should be taken into account in the estimation of the uncertainty produced by all systematic effects in 2018. We would like to emphasize that the 2018 observations campaign is expected to reduce this possible bias.

Continued monitoring of S0-2 beyond 2018 provides further opportunities to observe other relativistic effects, such as the advance of the periastron. The impact that a plausible binary system would have on these relativistic measurements is left for further work.

REFERENCES

Alexander, T. 2005, Physics Reports, 419, 65
Angélil, R. & Saha, P. 2010, ApJ, 711, 157
—. 2011, ApJ, 734, L19
Astropy Collaboration, Robitaille, T. P., Tollerud, E. J., Greenfield, P., Droettboom, M., Bray, E., Aldcroft, T., Davis, M., Ginsburg, A., Price-Whelan, A. M., Kerzendorf, W. E., Conley, A., Crighton, N., Barbary, K., Muna, D., Ferguson, H., Grollier, F., Parikh, M. M., Nair, P. H., Unther, H. M., Deil, C., Woillez, J., Conseil, S., Kramer, R., Turner, J. E. H., Singer, L., Fox, R., Weaver, B. A., Zabalza, V., Edwards, Z. I., Azalee Bostroem, K., Burke, D. J., Casey, A. R., Crawford, S. M., Dencheva, N., Ely, J., Jenness, T., Labrie, K., Lim, P. L., Pierfederici, F., Pontzen, A., Ptak, A., Refsdal, B., Servillat, M., & Streicher, O. 2013, A&A, 558, A33

Bartko, H., Martins, F., Trippe, S., Fritz, T. K., Genzel, R., Ott, T., Eisenhauer, F., Gillessen, S., Paumard, T., Alexander, T., Dodds-Eden, K., Gerhard, O., Levin, Y., Mascetti, L., Nayakshin, S., Perets, H. B., Perrin, G., Pfuhl, O., Reid, M. J., Rouan, D., Zilka, M., & Sternberg, A. 2009, The Astrophysical Journal, 708, 834
Boehle, A., Ghez, A. M., Schödel, R., Meyer, L., Yelda, S., Albers, S., Martinez, G. D., Becklin, E. E., Do, T., Lu, J. R., Matthews, K., Morris, M. R., Sitarski, B., & Witzel, G. 2016, ApJ, 830, 17
Borka, D., Jovanović, P., Borka Jovanović, V., & Zakharov, A. F. 2013, J. Cosmology Astropart. Phys., 11, 50
Chen, X. & Amaro-Seoane, P. 2014, The Astrophysical Journal, 786, L14
Do, T., Ghez, A. M., Morris, M. R., Lu, J. R., Matthews, K., Yelda, S., & Larkin, J. 2009, The Astrophysical Journal, 703, 1323

Do, T., Lu, J. R., Ghez, A. M., Morris, M. R., Yelda, S., Martinez, G. D., Wright, S. A., & Matthews, K. 2013, The Astrophysical Journal, 764, 154

Dworetsky, M. M. 1983, MNRAS, 203, 917

Eisenhauer, F., Genzel, R., Alexander, T., Abuter, R., Paumard, T., Ott, T., Gilbert, A., Gillessen, S., Horrobin, M., Trippe, S., Bonnet, H., Dumas, C., Hubin, N., Kaufer, A., Kissler Patig, M., Monnet, G., Strobele, S., Szeifert, T., Eckart, A., Schödel, R., & Zucker, S. 2005, The Astrophysical Journal, 628, 246

Feroz, F. & Hobson, M. P. 2008, Monthly Notices of the Royal Astronomical Society, 384, 449

Feroz, F., Hobson, M. P., & Bridges, M. 2009, MNRAS, 398, 1601

Feroz, F., Hobson, M. P., Cameron, E., & Pettitt, A. N. 2013, ArXiv e-prints

Ghez, A. M., Duchêne, G., Matthews, K., Hornstein, S. D., Tanner, A., Larkin, J., Morris, M., Becklin, E. E., Salim, S., Kremenek, T., Thompson, D., Soifer, B. T., Neugebauer, G., & McLean, I. 2003, The Astrophysical Journal, 586, L127

Ghez, A. M., Salim, S., Hornstein, S. D., Tanner, A., Lu, J. R., Morris, M., Becklin, E. E., & Duchêne, G. 2005, The Astrophysical Journal, 620, 744

Ghez, A. M., Salim, S., Weinberg, N. N., Lu, J. R., Do, T., Dunn, J. K., Matthews, K., Morris, M., Yelda, S., Becklin, E. E., Kremenek, T., Milosavljevic, M., & Naiman, J. 2008, ApJ, 1

Gillessen, S., Eisenhauer, F., Fritz, T. K., Bartko, H., Dodds-Eden, K., Pfuhl, O., Ott, T., & Genzel, R. 2009a, The Astrophysical Journal, 707, L114

Gillessen, S., Eisenhauer, F., Trippe, S., Alexander, T., Genzel, R., Martins, F., & Ott, T. 2009b, The Astrophysical Journal, 692, 1075

Gillessen, S., Plewa, P. M., Eisenhauer, F., Sari, R., Waisberg, I., Habibi, M., Pfuhl, O., George, E., Dexter, J., von Fellenberg, S., Ott, T., & Genzel, R. 2017, The Astrophysical Journal, 837, 30

Habibi, M., Gillessen, S., Martins, F., Eisenhauer, F., Plewa, P. M., Pfuhl, O., George, E., Dexter, J., Waisberg, I., Ott, T., von Fellenberg, S., Bauböck, M., Jimenez-Rosales, A., & Genzel, R. 2017, ApJ, 847, 120

Hees, A., Do, T., Ghez, A. M., Martinez, G. D., Naoz, S., Becklin, E. E., Boehle, A., Chappell, S., Chu, D., Dehghanfar, A., Kosmo, K., Lu, J. R., Matthews, K., Morris, M. R., Sakai, S., Schödel, R., & Witzel, G. 2017, Phys. Rev. Lett., 118, 211101

Hees, A., Ghez, A. M., Do, T., Lu, J. R., Morris, M. R., Becklin, E. E., Witzel, G., Boehle, A., Chappell, S., Chen, Z., Chu, D., Ciurlo, A., Dehghanfar, A., Gallego-Cano, E., Gautam, A., Jia, S., Kosmo, K., Martinez, G. D., Matthews, K., Naoz, S., Sakai, S., & Schödel, R. 2017, ArXiv e-prints

Hilditch, R. W. 2001, An Introduction to Close Binary Stars, 392

Hills, J. G. 1988, Nature, 331, 687

Hopman, C. 2009, The Astrophysical Journal, 700, 1933

Iorio, L. 2017, MNRAS, 472, 2249

Johannsen, T. 2016a, Classical and Quantum Gravity, 33, 113001

—. 2016b, Classical and Quantum Gravity, 33, 124001

Kerr, F. J. & Lynden-Bell, D. 1986, MNRAS, 221, 1023

Larkin, J., Barczys, M., Krabbe, A., Adkins, S., Aliado, T., Amico, P., Brims, G., Campbell, R., Canfield, J., Gasaway, T., Honey, A., Iserlohe, C., Johnson, C., Kress, E., LaFreniere, D., Magnone, K., Magnone, N., McElwain, M., Moon, J., Quirrenbach, A., Skulason, G., Song, I., Spencer, M., Weiss, J., & Wright, S. 2006, New A Rev., 50, 362

Levin, Y. 2007, Monthly Notices of the Royal Astronomical Society, 374, 515

Li, G., Ginsburg, I., Naoz, S., & Loeb, A. 2017, ArXiv e-prints

Löckmann, U., Baumgardt, H., & Kroupa, P. 2008, The Astrophysical Journal, 683, L151

Lomb, N. R. 1976, Ap&SS, 39, 447

Lu, J. R., Ghez, A. M., Hornstein, S. D., Morris, M. R., Becklin, E. E., & Matthews, K. 2009, The Astrophysical Journal, 690, 1463

Madigan, A.-M., Pfuhl, O., Levin, Y., Gillessen, S., Genzel, R., & Perets, H. B. 2014, The Astrophysical Journal, 784, 23

Martins, F., Gillessen, S., Eisenhauer, F., Genzel, R., Ott, T., & Trippe, S. 2008, The Astrophysical Journal, 672, L119

Martins, F., Trippe, S., Paumard, T., Ott, T., Genzel, R., Rauw, G., Eisenhauer, F., Gillessen, S., Maness, H., & Abuter, R. 2006, ApJ, 649, L103

Merritt, D., Gualandris, A., & Mikkola, S. 2009, ApJ, 693, L35

Morris, M. 1993, The Astrophysical Journal, 408, 496

Naoz, S. 2016, ARA&A, 54, 441

Ott, T., Eckart, A., & Genzel, R. 1999, The Astrophysical Journal, 523, 248

Paumard, T., Genzel, R., Martins, F., Nayakshin, S., Beloborodov, A. M., Levin, Y., Trippe, S., Eisenhauer, F., Ott, T., Gillessen, S., Abuter, R., Cuadra, J., Alexander, T., & Sternberg, A. 2006, The Astrophysical Journal, 643, 1011

Perets, H. B., Gualandris, A., Kupi, G., Merritt, D., & Alexander, T. 2009, ApJ, 702, 884

Perets, H. B., Hopman, C., & Alexander, T. 2007, The Astrophysical Journal, 656, 709

Pfuhl, O., Alexander, T., Gillessen, S., Martins, F., Genzel, R., Eisenhauer, F., Fritz, T. K., & Ott, T. 2014, The Astrophysical Journal, 782, 101

Phifer, K., Do, T., Meyer, L., Ghez, A. M., Witzel, G., Yelda, S., Boehle, A., Lu, J. R., Morris, M. R., Becklin, E. E., & Matthews, K. 2013, The Astrophysical Journal Letters, 773, L13

Psaltis, D., Wex, N., & Kramer, M. 2016, ApJ, 818, 121

Rafelski, M., Ghez, A. M., Hornstein, S. D., Lu, J. R., & Morris, M. 2007, The Astrophysical Journal, 659, 1241

Rubilar, G. F. & Eckart, A. 2001, A&A, 374, 95

Sana, H., de Mink, S. E., de Koter, A., Langer, N., Evans, C. J., Gieles, M., Gosset, E., Izzard, R. G., Le Bouquin, J.-B., & Schneider, F. R. N. 2012, Science, 337, 444

Scargle, J. D. 1982, The Astrophysical Journal, 263, 835

Stellingwerf, R. F. 1972, A&A, 21, 91

Stephan, A. P., Naoz, S., Ghez, A. M., Witzel, G., Sitarski, B. N., Do, T., & Kocsis, B. 2016, Monthly Notices of the Royal Astronomical Society, 460, 3494

Will, C. M. 2008, ApJ, 674, L25

Witzel, G., Ghez, A. M., Morris, M. R., Sitarski, B. N., Boehle, A., Naoz, S., Campbell, R., Becklin, E. E., Canalizo, G., Chappell, S., Do, T., Lu, J. R., Matthews, K., Meyer, L., Stockton, A., Wizinowich, P., & Yelda, S. 2014, ApJ, 796, L8

Witzel, G., Sitarski, B. N., Ghez, A. M., Morris, M. R., Hees, A., Do, T., Lu, J. R., Naoz, S., Boehle, A., Martinez, G., Chappell, S., Schödel, R., Meyer, L., Yelda, S., Becklin, E. E., & Matthews, K. 2017, The Astrophysical Journal, 847, 80

Yu, Q. & Tremaine, S. 2003, ApJ, 599, 1129

Zakharov, A. F., Jovanović, P., Borka, D., & Borka Jovanović, V. 2016, J. Cosmology Astropart. Phys., 05, 045

Zucker, S., Alexander, T., Gillessen, S., Eisenhauer, F., & Genzel, R. 2006, ApJ, 639, L21

TABLE 3
S0-2 Radial Velocity Measurements

UT	MJD	Epoch [a]	RV_{obs} (km s^{-1})	$RV\ \sigma$ (km s^{-1})	V_{LSR} [b] (km s^{-1})	RV_{LSR} [c] (km s^{-1})	RV [d] Source	Model (km s^{-1})	Model σ (km s^{-1})	Residual [e] (km s^{-1})
2000-06-23	51718.50	2000.476	1192	100	7	1199	(2)	1152	15	47
2002-06-02	52427.50	2002.418	-513	36	18	-495	(2)	-486	28	-9
2002-06-03	52428.50	2002.420	-550	44	18	-532	(2)	-554	27	22
2003-04-09	52739.23	2003.271		59		-1571	(3)	-1592	12	21
2003-05-09	52769.18	2003.353		40		-1512	(3)	-1547	11	35
2003-06-08	52798.50	2003.433	-1556	22	15	-1541	(2)	-1507	10	-34
2003-06-12	52803.15	2003.446		51		-1428	(3)	-1500	10	72

TABLE 3 — *Continued*

UT	MJD	Epoch [a]	$RV_{\rm obs}$ (km s^{-1})	RV σ (km s^{-1})	$V_{\rm LSR}$ [b] (km s^{-1})	$RV_{\rm LSR}$ [c] (km s^{-1})	RV [d] Source	Model (km s^{-1})	Model σ (km s^{-1})	Residual [e] (km s^{-1})
2004-06-23	53179.50	2004.476	-1151	57	8	-1143	(2)	-1121	7	-22
2004-07-14	53200.91	2004.535		46		-1055	(3)	-1104	7	49
2004-07-15	53201.64	2004.537		37		-1056	(3)	-1104	7	48
2004-08-18	53236.34	2004.632 [f]		39		-1039	(3)	-1078	7	39
2005-02-26	53428.46	2005.158		77		-1001	(3)	-948	6	-53
2005-03-18	53448.18	2005.212		37		-960	(3)	-936	6	-24
2005-03-19	53449.28	2005.215		54		-910	(3)	-935	6	25
2005-05-30	53520.50	2005.410	-945	23	19	-926	(2)	-893	6	-33
2005-06-15	53536.94	2005.455		60		-839	(3)	-884	6	45
2005-06-17	53539.13	2005.461		43		-907	(3)	-882	6	-25
2005-07-03	53554.50	2005.503	-845	34	3	-842	(2)	-874	6	32
2005-09-04	53618.02	2005.677 [f]		77		-774	(3)	-838	6	64
2005-10-08	53651.63	2005.769 [f]		58		-860	(3)	-820	6	-40
2006-03-15	53810.51	2006.204		42		-702	(3)	-739	5	37
2006-04-21	53847.40	2006.305		77		-718	(3)	-721	5	3
2006-05-23	53878.50	2006.390	-715	21	23	-692	(2)	-707	5	14
2006-06-18	53904.50	2006.461	-728	17	10	-718	(2)	-694	5	-24
2006-06-30	53916.50	2006.494	-699	36	4	-695	(2)	-689	5	-6
2006-07-01	53917.50	2006.497	-717	37	4	-713	(2)	-688	5	-25
2006-08-16	53963.92	2006.624 [f]		57		-658	(3)	-667	5	9
2007-03-25	54185.26	2007.230		57		-586	(3)	-570	5	-16
2007-04-21	54212.29	2007.304		57		-537	(3)	-558	5	21
2007-05-21	54241.50	2007.384	-507	50	24	-483	(2)	-546	5	63
2007-07-19	54300.29	2007.545	-502	50	-4	-506	(2)	-522	5	16
2007-07-20	54302.14	2007.550 [f]		57		-505	(3)	-521	5	16
2007-09-03	54347.06	2007.673 [f]		57		-482	(3)	-503	4	21
2008-04-05	54562.20	2008.262 [f]		27		-394	(3)	-418	4	24
2008-05-16	54602.50	2008.372	-443	32	26	-417	(2)	-402	4	-15
2008-06-06	54623.92	2008.431		62		-425	(3)	-394	4	-31
2008-07-25	54672.28	2008.563	-373	43	-7	-380	(2)	-375	4	-5
2009-05-05	54956.50	2009.342	-282	30	30	-252	(2)	-268	4	17
2009-05-06	54957.50	2009.344	-315	32	30	-285	(2)	-268	4	-17
2009-05-20	54972.37	2009.385		45		-241	(3)	-262	4	21
2010-05-08	55324.50	2010.349	-152	22	29	-123	(2)	-131	4	9
2010-05-09	55326.30	2010.354		27		-134	(3)	-131	4	-3
2011-04-26	55678.03	2011.317		34		-3	(3)	3	3	-6
2011-07-10	55752.33	2011.520	14	23	0	14	(2)	32	3	-19
2011-07-26	55769.35	2011.567		57		35	(3)	39	3	-4
2012-03-17	56004.20	2012.210		34		185	(3)	135	3	50
2012-05-04	56052.42	2012.342		34		167	(3)	155	3	12
2012-06-08	56086.50	2012.435	128	25	15	143	(2)	169	3	-26
2012-06-09	56087.46	2012.438	141	34	14	155	(2)	170	3	-15
2012-06-11	56089.50	2012.444	151	50	13	164	(2)	171	3	-6
2012-06-29	56107.93	2012.494		34		195	(3)	179	3	16
2012-07-06	56114.87	2012.513		34		186	(3)	182	3	4
2012-07-21	56129.31	2012.553	178	56	-6	172	(2)	188	3	-16
2012-07-22	56130.31	2012.555	200	8	-6	194	(2)	188	3	6
2012-08-12	56151.33	2012.613	213	25	-13	200	(2)	197	3	2
2012-08-13	56152.27	2012.615	199	24	-14	186	(2)	198	3	-12
2012-09-14	56185.00	2012.705		45		190	(3)	212	3	-22
2013-04-05	56388.45	2013.262		23		313	(3)	306	3	7
2013-05-11	56423.50	2013.358	295	38	28	323	(1)	323	3	-0
2013-05-12	56424.50	2013.361	298	22	27	325	(1)	323	3	2
2013-05-13	56425.50	2013.363	251	39	27	278	(1)	324	3	-46
2013-05-14	56426.50	2013.366	272	16	27	298	(2)	324	3	-26
2013-05-16	56428.50	2013.372	286	24	26	311	(2)	325	3	-14
2013-05-17	56429.50	2013.374	287	30	25	312	(1)	326	3	-13
2013-07-25	56498.33	2013.563	367	15	-7	360	(2)	360	4	1
2013-07-26	56499.34	2013.566	366	39	-7	359	(2)	360	4	-2
2013-07-27	56500.33	2013.568	367	39	-8	360	(2)	361	4	-1
2013-08-10	56514.29	2013.607	393	32	-13	380	(2)	368	4	12
2013-08-11	56515.31	2013.609	354	40	-13	341	(2)	368	4	-27
2013-08-13	56517.29	2013.615	353	44	-14	340	(2)	369	4	-30
2013-08-27	56531.99	2013.655		45		361	(3)	377	4	-16
2013-09-22	56557.92	2013.726		34		384	(3)	390	4	-6
2014-03-08	56725.57	2014.185		28		490	(3)	481	4	9
2014-04-06	56754.06	2014.263		34		515	(3)	497	4	18
2014-05-17	56795.50	2014.376	481	32	25	506	(1)	522	4	-16
2014-05-22	56800.50	2014.390	500	33	23	523	(1)	525	4	-2
2014-07-02	56841.36	2014.502	553	15	3	556	(1)	550	4	6
2014-07-09	56848.30	2014.521		17		568	(3)	554	4	14
2015-04-19	57132.46	2015.299		23		765	(3)	751	5	14
2015-05-03	57146.50	2015.337	743	28	31	774	(1)	762	5	12

TABLE 3 — *Continued*

UT	MJD	Epoch[a]	RV_{obs} (km s^{-1})	$RV\ \sigma$ (km s^{-1})	V_{LSR}[b] (km s^{-1})	RV_{LSR}[c] (km s^{-1})	RV[d] Source	Model (km s^{-1})	Model σ (km s^{-1})	Residual[e] (km s^{-1})
2015-07-20	57224.35	2015.551	829	41	-5	823	(1)	826	5	-3
2015-09-15	57281.12	2015.706		45		869	(3)	877	5	-8
2016-04-13	57492.23	2016.284		45		1081	(3)	1100	8	-19
2016-05-14	57522.50	2016.367	1081	36	26	1107	(1)	1138	8	-31
2016-05-15	57523.50	2016.370	1139	33	26	1165	(1)	1140	8	26
2016-05-16	57524.50	2016.372	1117	16	26	1142	(1)	1141	8	1
2016-07-08	57578.06	2016.519		34		1198	(3)	1214	9	-16

[a] The epoch time is reported in Julian years 365.25 days since J2000.

[b] The values came from *rvcorrect* task in IRAF, with an error less than 1 km s^{-1}(Kerr & Lynden-Bell 1986). For ease of viewing, values have been rounded.

[c] Velocity after applying the V_{LSR} correction. For ease of viewing, values have been rounded.

[d] Measurement reported in (1) this work, (2) Boehle et al. (2016) and (3) Gillessen et al. (2017).

[e] $RV_{\text{LSR}} -$ model. For ease of viewing, values have been rounded.

[f] VLT combined nights data.

APPENDIX

ORBITAL FIT

The model for S0-2's long-term RV variation is based on a joint orbital fit of S0-2 and S0-38. We used the same S0-2 and S0-38 astrometry[6] and process as Boehle et al. (2016), S0-38 RV from (Gillessen et al. 2017), but with the S0-2 RVs from Table 3. It should also be noted that the impact of S0-38 is negligible for this S0-2 binary study. The resulting orbital parameters are listed in Table 4, with all results being consistent with Boehle et al. (2016) within 1σ.

TABLE 4
RESULTS FROM ORBITAL FIT

Model Parameter (units)	Parameter Value [a]
Black Hole Properties:	
Distance (kpc)	$7.93 \pm 0.13 \pm 0.04$
Mass (10^6 $M_\odot$)	$4.03 \pm 0.14 \pm 0.04$
X position of Sgr A* (mas)	$2.17 \pm 0.47 \pm 1.90$
Y position of Sgr A* (mas)	$-4.31 \pm 0.60 \pm 1.23$
X velocity (mas yr^{-1})	$-0.11 \pm 0.03 \pm 0.13$
Y velocity (mas yr^{-1})	$0.67 \pm 0.06 \pm 0.22$
Z velocity (km s^{-1})	$-9.99 \pm 6.25 \pm 4.28$
S0-2 Properties:	
Period (yr)	15.92 ± 0.04
Time of closest approach (yr)	2018.266 ± 0.04
Eccentricity	0.892 ± 0.002
Inclination (deg)	134.3 ± 0.3
Arguement of periapse (deg)	66.7 ± 0.5
Angle of the ascending node (deg)	228.0 ± 0.5
S0-38 Properties:	
Period (yr)	19.20 ± 0.2
Time of closest approach (yr)	2003.1 ± 0.04
Eccentricity	0.811 ± 0.004
Inclination (deg)	170 ± 2
Arguement of periapse (deg)	194 ± 160
Angle of the ascending node (deg)	79 ± 24

[a] The first error term for each best-fit value corresponds to the statistical error determined by the orbital fit. For the black hole parameters, the second error term corresponds to jackknife uncertainty from the reference frame, which were reported in Boehle et al. (2016).

LOMB-SCARGLE METHOD

In this work, we used the Lomb-Scargle method to look for periodic signals in the S0-2 data. The Lomb-Scargle method works best at detecting sinusoidal signals, which corresponds to a circular binary system. However, as binaries become eccentric, their radial velocity curve deviates more from a perfect sine wave. Although their curves are periodic, their non-sinusoidal shapes could lead to reduced sensitivity using the Lomb-Scargle periodogram.

We explored the method's sensitivity to eccentricity by generating four sets of 100,000 simulated eccentric binary radial velocity curves (see equation 3). The first set of curves had $e = 0$, the second set had $e = 0.25$, the third set had $e = 0.5$ and the fourth set had $e = 0.9$. All curves had the same period of 10 days, a K value of 30 km s^{-1}, and ω of 0 degrees (Figure 6). These curves were also sampled at the same times as our data. We ran each set of curves through the Lomb-Scargle analysis and took the median power values for each period. The Lomb-Scargle method successfully identified the 10 days period in the different sets of simulated curves. The median power values at the 10 days period varied by less than 0.04 between the sets. We interpret the second peak as a product of the sampling of our observations.

We did this same analysis but instead kept the RV amplitude constant at 30 km s^{-1}, where RV amplitude is defined as $(RV_{\max} - RV_{\min})/2$. To do this, we changed the value of K for each value of eccentricty, which corresponds to changing the semi-major axis since the period remains constant at 10 days (Figure 7). We find that the Lomb-Scargle power at 10 days for the different eccentricities differ by less than 0.07 for eccentricities of 0, 0.25, and 0.5. For an eccentricity of 0.9, the power value drops to 0.11 at 10 days. We again interpret the second peak as a product of the sampling of our observations.

[6] We do not report new astrometric measurements, as additional astrometric data is not expected to significantly affect S0-2's RV curve.
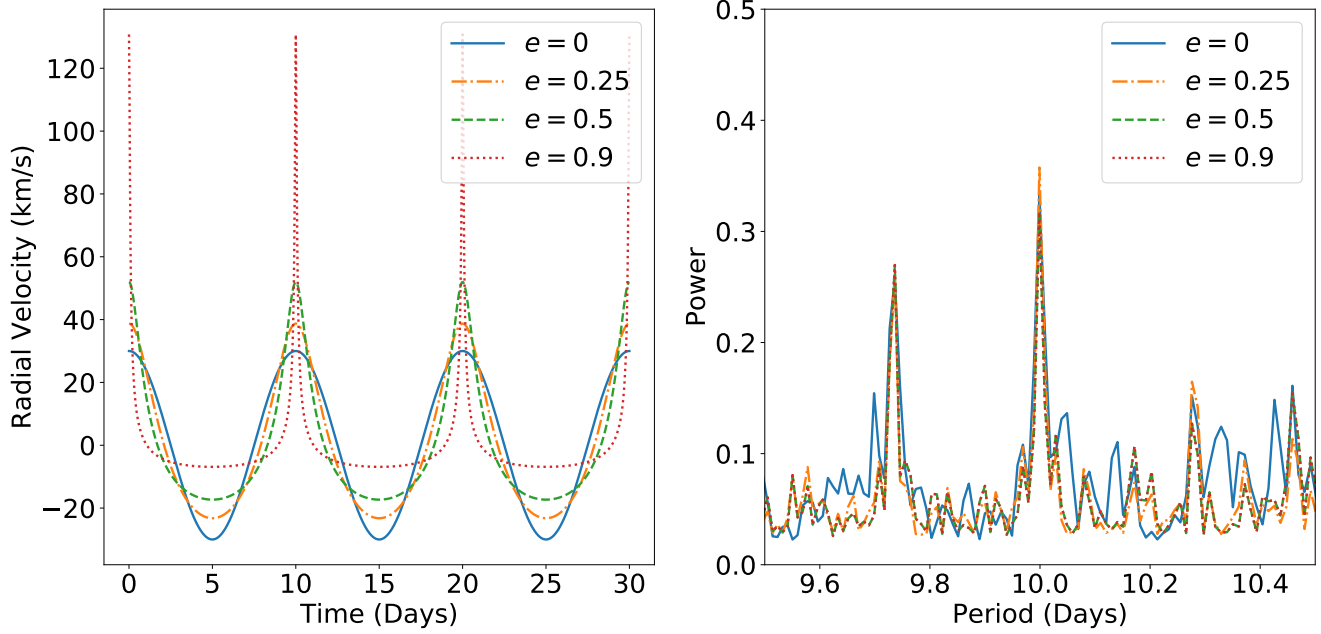
FIG. 6.— Left: Sample radial velocity curves with different eccentricities. Each curve has a period of 10 days, a K value of 30 km s^{-1} and ω of 0 degrees. Each curve was sampled at the same times as our data. Right: Median Lomb-Scargle power values for each set of 100,000 simulations run for the different eccentric curves.
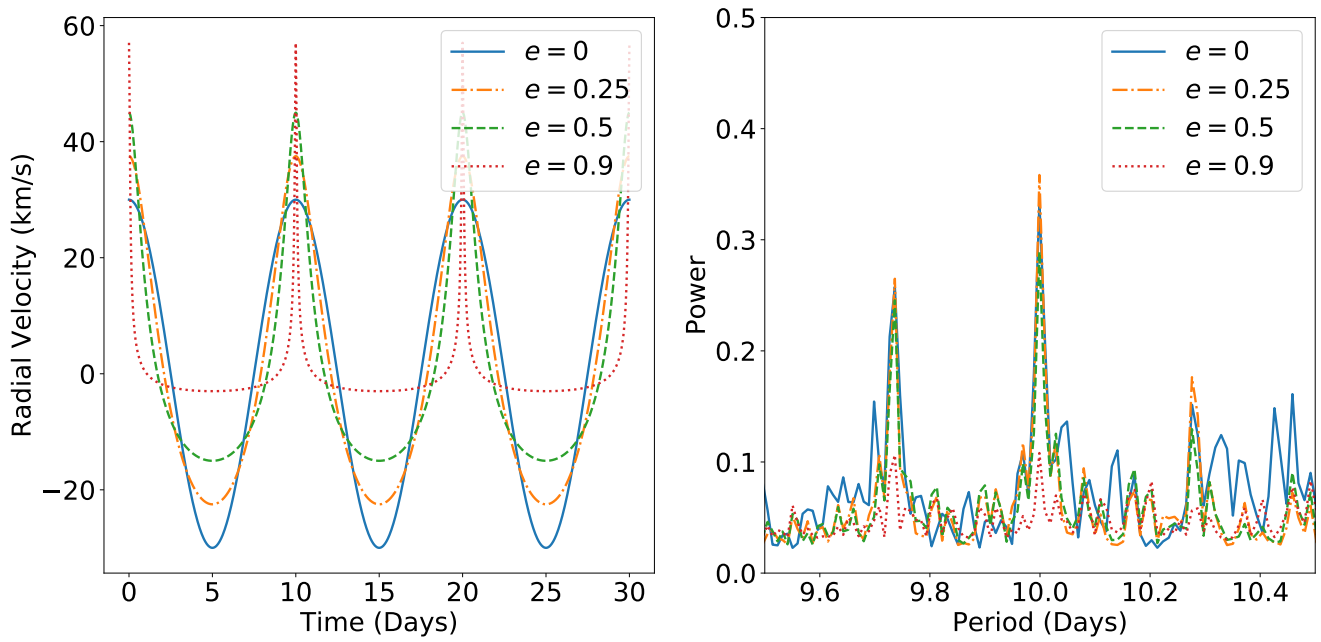

FIG. 7.— Left: Sample radial velocity curves with different eccentricities. Each curve has a period of 10 days, a RV amplitude of 30 km s^{-1} and ω of 0 degrees. Each curve was sampled at the same times as our data. Right: Median Lomb-Scargle power values for each set of 100,000 simulations run for the different eccentric curves.